

Scaling Behavior of the Heisenberg Model in Three Dimensions

A. Gordillo-Guerrero^{1,2}, *R. Kenna*³ and *J.J. Ruiz-Lorenzo*^{4,2}

¹ Departamento de Ingeniería Eléctrica, Electrónica y Automática,
Universidad de Extremadura, Avda Universidad s/n,
Cáceres, 10071, Spain.

² Instituto de Biocomputación and
Física de Sistemas Complejos (BIFI),
Zaragoza, 50009, Spain.

³ Applied Mathematics Research Centre,
Coventry University, Coventry, CV1 5FB, England

⁴ Departamento de Física,
Universidad de Extremadura, Avda Elvas s/n,
Badajoz, 06071, Spain.

June 10, 2021

Abstract

We report on extensive numerical simulations of the three-dimensional Heisenberg model and its analysis through finite-size scaling of Lee-Yang zeros. Besides the critical regime, we also investigate scaling in the ferromagnetic phase. We show that, in this case of broken symmetry, the corrections to scaling contain information on the Goldstone modes. We present a comprehensive Lee-Yang analysis, including the density of zeros and confirm recent numerical estimates for critical exponents.

1 Introduction

The universality concept is commonly stated together with the hypotheses of scaling and finite-size scaling for thermodynamic functions close to the critical points associated with continuous phase transitions. The theory of finite-size scaling has been mostly successful in determining critical and non-critical properties of bulk systems from those of their finite or partially finite counterparts [1]. Although comparisons between theory and experiment, as well as between the variety of theoretical approaches, yield good overall agreement in the main, difficulties in reconciling details of scaling in a number of important systems remain [2, 3]. These include some systems with continuous symmetry groups, such as the those in the three-dimensional $O(3)$ Heisenberg universality class. Experimental realizations of this model include isotropic ferromagnets with and without quenched disorder, e.g. Ni, EuO and $\text{La}_{1-x}\text{A}_x\text{MnO}_3$. Precise theoretical estimates for the critical temperature and critical exponents are contained in Refs.[4, 5] for the pure and site-diluted Heisenberg models with quenched disorder. A review of theoretical and experimental measurements of critical exponents for the Heisenberg model is contained in Ref. [6].

Here we study the Heisenberg model in three dimensions. Our objective is not to revisit old ground but to investigate, for the first time, the Lee-Yang zeros of this continuous-symmetry-group model through Monte Carlo simulations [7]. We do this through finite-size scaling, primarily at the critical point, but also in the ferromagnetic regime. One motivation is to investigate the Goldstone modes in the broken phase, which affect the corrections to scaling there. The symmetric phase manifests the Yang-Lee edge, which also has not previously been analyzed numerically in this model. We also investigate the crossover in behavior of the density of zeros from the critical point to the ferromagnetic phase.

In the next section we outline the Heisenberg model and briefly discuss the observables we focus on in this paper. In Section 3 we give details of the Monte Carlo simulations. The outcomes of the simulations are analyzed in Section 4. A compact scaling description in terms of densities of zeros is given in Section 5 and we conclude in Section 6.

2 Model and observables

The Heisenberg model in d dimensions may be defined in terms of $O(3)$ spin variables placed at the nodes of a cubic lattice. The volume of the lattice is $V = L^d$ where L is its linear size and the lattice constant has been set to one. The model is governed by a Hamiltonian \mathcal{H} given by

$$\beta\mathcal{H} = -\beta \sum_{\langle i,j \rangle} \mathbf{S}_i \cdot \mathbf{S}_j - \mathbf{h} \cdot \sum_i \mathbf{S}_i. \quad (2.1)$$

Here $\beta = 1/(k_B T)$, where T is the temperature and \mathbf{h} is an external magnetic field. The \mathbf{S}_i are three-dimensional vectors of unit modulus and the first sum is extended only over nearest neighbors. We henceforth set the Boltzmann constant k_B to unity. We define the

total nearest-neighbor energy as

$$E = - \sum_{\langle i,j \rangle} \mathbf{S}_i \cdot \mathbf{S}_j \quad (2.2)$$

and the total magnetization density as a three-component vector

$$\mathbf{M} = (M_x, M_y, M_z) = \sum_i \mathbf{S}_i. \quad (2.3)$$

The partition function is

$$Z_L(T, h) = \sum_{\{\mathbf{S}_i\}} \exp(-\beta \mathcal{H}) = \sum_{\{\mathbf{S}_i\}} \exp(-\beta E + \mathbf{h} \cdot \mathbf{M}). \quad (2.4)$$

The susceptibility is defined through the derivatives

$$\nabla_h \ln Z = \frac{1}{V} \langle \mathbf{M} \rangle, \quad (2.5)$$

$$\chi_L(T, h) = \frac{1}{V} \nabla_h^2 \ln Z_L(T, h) = \frac{1}{V} (\langle \mathbf{M}^2 \rangle - \langle \mathbf{M} \rangle^2), \quad (2.6)$$

in which the thermal average is denoted by $\langle \dots \rangle$. Because the probability of reaching every minimal value for the free energy is non-vanishing, the thermal average of Eq. (2.3) is zero in the absence of an external field, for a finite lattice. While this is an accurate finite-size counterpart for the susceptibility in the symmetric phase, it cannot be used to capture the connected susceptibility in the broken phase. Therefore we have to introduce separate definitions for the connected and non-connected finite-size susceptibilities, namely

$$\tilde{\chi}_L(T, h = 0) = \frac{1}{V} (\langle \mathbf{M}^2 \rangle - \langle |\mathbf{M}| \rangle^2), \quad (2.7)$$

and

$$\chi_L^{(\text{nc})}(T, h = 0) = \frac{1}{V} \langle \mathbf{M}^2 \rangle. \quad (2.8)$$

For numerical measurements on a finite lattice it is appropriate to use $\tilde{\chi}_L$ and $\chi_L^{(\text{nc})}$ in the ferromagnetic and paramagnetic regimes, respectively. One should not use $\tilde{\chi}_L$ in the paramagnetic phase because, unlike $\langle \mathbf{M} \rangle$, $\langle |\mathbf{M}| \rangle$ does not vanish there for finite-size systems. Indeed, the usage of $\langle |\mathbf{M}| \rangle$ in the symmetric phase would be tantamount to the introduction of a non-vanishing external field there. There is no order parameter for finite-size systems (because they do not manifest a phase transition), but $\chi_L^{(\text{nc})}$ and $\tilde{\chi}_L$ each approach χ_∞ in the thermodynamic limit.

Inspired by the fundamental theorem of algebra, Lee and Yang introduced the idea of complex zeros of the partition function as a way to investigate the onset and properties of phase transitions [7]. The resulting approach constitutes a fundamental theory of phase transitions [8]. In the paramagnetic phase, the Lee-Yang zeros in the complex h -plane remain away from the real magnetic-field axis, as proved in Ref.[9]. This means there exists a gap on the imaginary h -axis in which the density of zeros is zero. The free energy

is analytic in h in the gap and no phase transition can occur as a function of h . The ends of the non-vanishing distribution of zeros was termed the Yang-Lee edge in Ref. [10]. The proof that the Lee-Yang zeros of the partition function are located on the imaginary h -axis for the Heisenberg ferromagnet was given in Ref. [11]. Here we present a numerical investigation into the Lee-Yang zeros for the model in three dimensions.

Following Ref.[12], for example, in order to find the Lee-Yang (LY) zeros of the system we write the partition function in an imaginary field of strength ir as

$$Z_L(T, ir) = Z_L(T, 0)\langle \cos(rM) + i \sin(rM) \rangle, \quad (2.9)$$

where M is the component of \mathbf{M} picked out by the field. Here the thermal average is a real measure, taken with $Z(T, h = 0)$. Since the mean value of an observable which is not invariant under $O(3)$ is automatically zero, odd moments of the magnetization vanish. Therefore the partition function in a pure imaginary magnetic field is real and the zeros are given by $\langle \cos(rM) \rangle = 0$. In the ferromagnetic phase, and in analogy with Eq.(2.7), one may use for M the modulus $|\mathbf{M}|$. Then one seeks the zeros as solutions to

$$\langle \cos(r|\mathbf{M}|) \rangle = 0. \quad (2.10)$$

However, just as Eq.(2.7) is inappropriate in the high-temperature phase, so is Eq.(2.10) unsuitable there. Instead, and in analogy to Eq.(2.8), one has to use an explicit component for M , say $M = M_x$.

$$\langle \cos(rM_x) \rangle = 0. \quad (2.11)$$

In this way we can attempt to obtain the zeros of the partition function for each L in the various regimes. The resulting j th, temperature-dependent, Lee-Yang zero is denoted by $r_j(T; L)$, the zero with $j = 1$ being the smallest.

2.1 Scaling of the thermodynamic functions and zeros

In the limit of infinite volume, the standard expressions for the leading thermal scaling are $\chi_\infty(T) \sim |t|^{-\gamma}$, $m_\infty(h) \sim h^{1/\delta}$, $\xi_\infty(T) \sim |t|^{-\nu}$ and $r_1(T) \sim t^\Delta$, for $t > 0$. Here, t is the reduced temperature, $(T - T_c)/T_c$, and we suppress writing explicit dependency on h or t when they vanish. In the following, we focus on the finite-size scaling (FSS) of the susceptibility and zeros. According to standard FSS theory, these are obtained through the substitution $\xi_\infty(T) \rightarrow \xi_L(T_c) \sim L$ or $t \rightarrow L^{-1/\nu}$. Therefore we expect to extract the leading scaling behavior through

$$\chi_L(T_c) \sim L^{\frac{\gamma}{\nu}}, \quad r_j(T_c; L) \sim L^{-\frac{\Delta}{\nu}}. \quad (2.12)$$

We can estimate γ/ν and Δ/ν through the scaling relations

$$\frac{\gamma}{\nu} = 2 - \eta, \quad \text{and} \quad \frac{\Delta}{\nu} = \frac{d + 2 - \eta}{2}, \quad (2.13)$$

provided the anomalous dimension η is known. The most recent measurement of this critical exponent is $\eta = 0.0391(9)$ [5] and from this one obtains

$$\frac{\gamma}{\nu} = 1.609(9) \quad \text{and} \quad \frac{\Delta}{\nu} = 2.4805(4). \quad (2.14)$$

These values will be used throughout this work.

2.2 Compact scaling of Lee-Yang zeros

In Ref.[13], it was suggested that the partition function zeros could scale, in the critical region, as a fraction of the total number of zeros, i.e., as a function of j/L^d , for large values of the index j . In fact many models give scaling in the ratio $(j - \epsilon)/L^d$ in which $\epsilon = 1/2$ [14, 15]. If such a functional form is widespread for Lee-Yang zeros, it suggests that Eq.(2.12) be promoted to the more comprehensive form

$$r_j(T; L) \sim \left(\frac{j - \epsilon}{L^d} \right)^{C(T)}, \quad (2.15)$$

for $T \leq T_c$. To investigate this further, first write the finite-size partition function in terms of its Lee-Yang zeros as

$$Z_L(T, h) = A \prod_{j=1}^{V/2} (h - h_j)(h - h_j^*), \quad (2.16)$$

where A is non-vanishing (as a function of h) and $*$ means complex conjugation. Then the susceptibility is

$$\chi_L(T) = -\frac{1}{V} \sum_{j=1}^{V/2} \left(\frac{1}{h_j^2} + \frac{1}{h_j^{*2}} \right). \quad (2.17)$$

When the Lee-Yang theorem [7] holds and $h_j = ir_j$ is purely imaginary this gives that

$$\chi_L(T) = \frac{2}{V} \sum_{j=1}^{V/2} \frac{1}{r_j^2(T; L)}. \quad (2.18)$$

Eq.(2.18) relates the Lee-Yang zeros to the susceptibility defined through Eq.(2.6), i.e., through the second derivative of the partition function. To gain insight into the behavior of the zeros away from criticality, we consider the $T \rightarrow 0$ and $T \rightarrow \infty$ limits of this susceptibility. For a finite-size system, the full susceptibility χ_L from Eq.(2.6) coincides with the non-connected version $\chi_L^{(\text{nc})}$ defined through Eq.(2.8), and at low temperatures, $\chi_L(T \ll 1) = \chi_L^{(\text{nc})}(T \ll 1) \simeq V$. If $T \rightarrow \infty$, on the other hand, $\chi_L(T \rightarrow \infty) = \chi_L^{(\text{nc})}(T \rightarrow \infty) = 1$. Note that, these are different to the modified susceptibility $\tilde{\chi}_L(T)$ as defined in Eq.(2.7). This is only used as a replacement for $\chi_L(T)$ below T_c and, in the low-temperature limit where the spins align, it is $\tilde{\chi}_L(T = 0) = 0$. However, even in the paramagnetic phase, it is the susceptibility χ_L (equivalently $\chi_L^{(\text{nc})}$), and not $\tilde{\chi}_L$ that is related to the Lee-Yang zeros through Eq.(2.18).

In the absence of a YL edge, when the zeros can pinch the real axis, we assume the form (2.15) for the comprehensive scaling of the zeros. Inserting into Eq.(2.18), one finds that the leading finite-size behavior of the susceptibility is

$$\chi_L(T) \sim L^{d(2C-1)}, \quad (2.19)$$

which comes from the contributions from the lowest zeros.

This recovers the FSS formula (2.12) in the critical regime provided $C(T_c) = \Delta/\nu d$. It also recovers the scaling $\chi_L(T < T_c) \sim L^d$ in the ferromagnetic phase if $C = 1$ there. The ansatz (2.15) fails in the paramagnetic phase, however, because, it does not take into account the Yang-Lee edge and, plugged into Eq.(2.18), it would lead to a spurious logarithmic divergence in the susceptibility there.

2.3 Corrections to scaling

At the critical point, the corrections to leading finite-size scaling are governed by the ω exponent. For the susceptibility and Lee-Yang zeros, one expects

$$\chi_L(T_c) \sim L^{\frac{\gamma}{\nu}} [1 + \mathcal{O}(L^{-\omega})], \quad (2.20)$$

$$r_j(T_c; L) \sim L^{-\frac{\Delta}{\nu}} [1 + \mathcal{O}(L^{-\omega})]. \quad (2.21)$$

The widely accepted measured value for the correction exponent is $\omega \approx 0.8$ [5, 6].

Away from the critical temperature one may also expect corrections to scaling. Since the model under consideration has continuous symmetry group, the effects of Goldstone modes in the ferromagnetic regime are of interest (the ferromagnetic phase is also critical). Since these modes are massless, the corresponding propagator is $1/p^2$ in momentum space, producing an L^2 divergence in the connected susceptibility. The longitudinal susceptibility on the other hand, diverges as $1/p^{4-d} = 1/p$, inducing a correction proportional to L . Therefore, the susceptibility for the Heisenberg model in the ferromagnetic phase (in the presence of Goldstone modes) may be expected to scale as

$$\chi_L(T < T_c) \sim L^3 [1 + \mathcal{O}(L^{-1}) + \mathcal{O}(L^{-2})]. \quad (2.22)$$

In the Ising case, on the other hand, the absence of Goldstone modes suggests the absence of such correction. There, one expects Eq.(2.22) to be replaced by $\chi_L(T < T_c) \sim L^3 [1 + \mathcal{O}(L^{-3})]$. Therefore the corrections to scaling in the broken phase deliver information on the existence of Goldstone modes. As we have seen, the Lee-Yang zeros are closely related to the susceptibility. They may therefore be expected to carry the same correction-to-scaling behavior. One then expects, for the zeros in the low-temperature phase,

$$r_j(T < T_c; L) \sim L^{-d} [1 + \mathcal{O}(L^{-1})]. \quad (2.23)$$

Combining with the index-dependency suggested in the previous subsection, one expects a comprehensive scaling behavior for the Lee-Yang zeros for the Heisenberg model as

$$r_j(T; L) = \left(\frac{j - \epsilon}{L^d} \right)^C [1 + \mathcal{O}(L^{-E})], \quad (2.24)$$

with $C = \Delta/\nu d$ and $E = \omega$ when $T \approx T_c$, and $C = 1$ and $E = 1$ when $T \ll T_c$.

3 Simulation details

We simulated the Heisenberg model on regular, cubic lattices with linear sizes $L = 8, 12, 16, 24, 32, 48$ and 64 . We used periodic boundary conditions and in each case 20

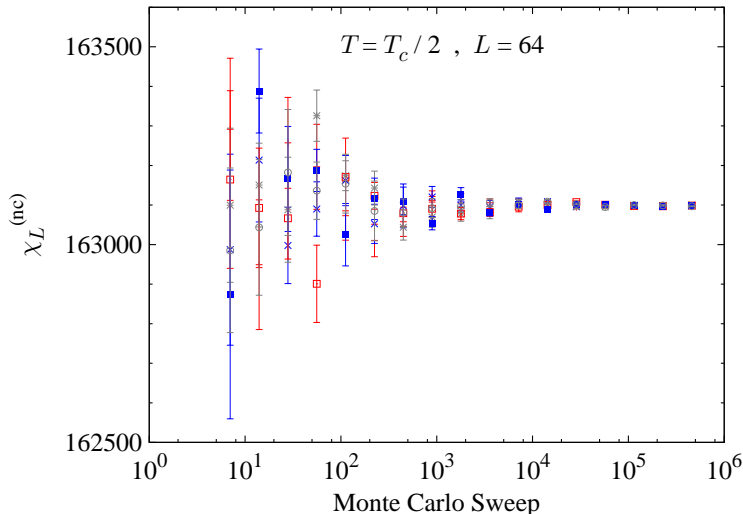


Figure 1: Log-binning of susceptibility for five random pseudosamples (in color online) with $L = 64$ simulated at $T = T_c/2$. Error bars are typical deviations in each bin. The first block only includes seven measurements, explaining the deviations for small times.

pseudosamples were used to average out the thermal noise. We performed our simulations at several different values of the system temperature. We use the estimate for the critical temperature $\beta_c = 1/T_c = 0.693$ from Ref. [16]. Apart from this value, we also simulated at two lower temperatures: $T = 2T_c/3$ ($\beta = 1.0395$) and $T = T_c/2$ ($\beta = 1.386$) both in ferromagnetic regime.

The update scheme involved the Metropolis method applied to over 10% of the individual spins, chosen at random, followed by a number (increasing with L) of cluster updates using a Wolff cluster method. See Table 1 for details. We refer to each one of these combined updates as a Monte Carlo sweep. After every Monte Carlo sweep we measure magnetization and energy, performing 10^6 measurements for every pseudosample.

In order to work with thermally equilibrated systems, we performed 10^5 Monte Carlo sweeps before starting measurements. We start the simulations from hot (random) distributions of the spin variables, although we have checked that the averages do not change if we begin with cold configurations (i.e., all spins pointing in the same direction). In Fig. 1, we compare the thermalization of the different pseudosamples in the most challenging case, i.e. our largest system at the lowest temperature. We performed a similar check for the log-binning of the specific heat.

L	8	12	16	24	32	48	64
N_{Wolff}	10	20	25	40	50	75	100

Table 1: The Monte Carlo sweep size for each system size L . Here, N_{Wolff} denotes the number of Wolff updates performed after the partial Metropolis update.

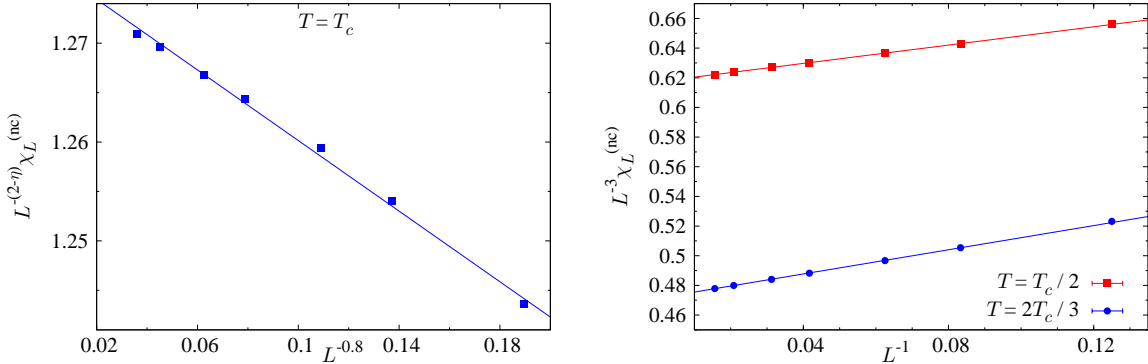


Figure 2: Finite-size scaling of the susceptibility at the critical point (left) and in the ferromagnetic regime (right), supporting the forms (2.20) and (2.22), respectively.

4 Finite-size scaling

We begin our analysis with a brief discussion of FSS of the susceptibility in the critical and ferromagnetic regimes. As mentioned in the introduction, our aim is not to generate new estimates for the critical temperature and critical exponents. Rather, we wish to examine previously under-researched aspects of the Heisenberg model. Therefore, we first check the consistency of our results with earlier studies before moving on to the Lee-Yang zeros, which form the focus for our work. In Fig. 2 (left panel), the critical susceptibility data are plotted with a best fit to Eq.(2.20). The estimates $\gamma/\nu = 1.609(9)$ and $\omega = 0.8$ from Ref. [5] are used. The fit confirms these estimates for the data. The susceptibility is also plotted in the ferromagnetic phase in Fig. 2 (right panel). The scaling form (2.22) is confirmed, including the corrections coming from the Goldstone modes.

To achieve relatively small error bars in estimating the zeros, we follow an iterative approach whereby we first estimate the location of the zeros by detecting changes in the sign of Eq.(2.10) using a relatively large interpolation step and, from this estimation, we restart the search with a smaller interpolation step. We terminate this iterative search

L	$r_1(L)$	$r_2(L)$	$r_3(L)$	$r_4(L)$
8	0.00825415(59)	0.0243727(17)	0.0396287(27)	0.0541716(40)
12	0.00300815(27)	0.00888260(73)	0.0144417(12)	0.0197404(21)
16	0.00147165(14)	0.00434424(34)	0.00706250(50)	0.0096533(9)
24	0.000537193(39)	0.00158625(11)	0.00257895(18)	0.0035250(3)
32	0.000262952(19)	0.000776455(47)	0.0012622695(74)	0.00172516(17)
48	0.0000960985(9)	0.000283759(24)	0.0004612664(37)	0.00063038(6)
64	0.0000470623(4)	0.000138962(10)	0.0002258879(16)	0.00030869(3)

Table 2: The first four Lee-Yang zeros for different lattice sizes at $T = T_c$.

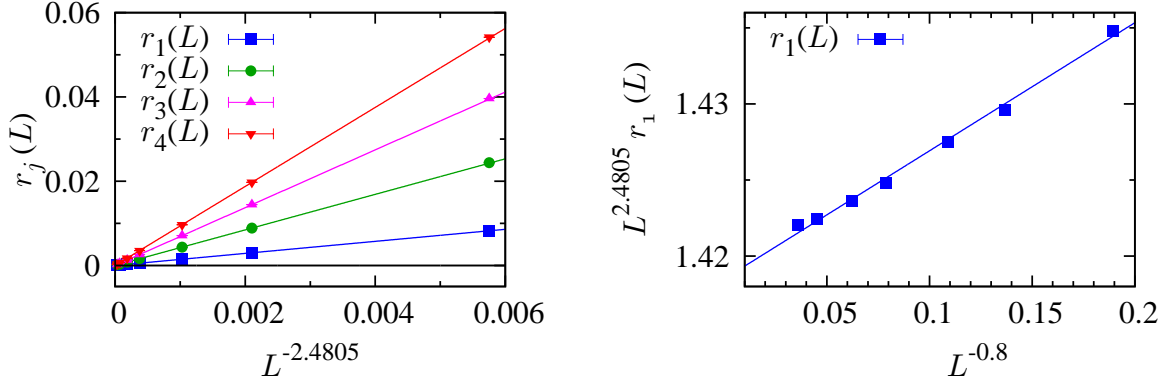


Figure 3: Scaling of the first four Lee-Yang zeros at the critical temperature (in color online). The left panel confirms the leading finite-size scaling at the critical point as $\chi_L(0) \sim L^{\Delta/\nu} = L^{-2.4805}$ following Eq.(2.20). The right panel lends support for the accepted value of the finite-size correction exponent $\omega = 0.8$.

once the error bars do not further decrease upon reducing the interpolation step size. The estimates for zeros at T_c and below T_c are listed in Tables 2, 3 and 4, respectively.

The scaling dependency of the zeros on the system size is obtained by fitting to

$$r_j(L) = a + bL^{-c}(1 + fL^{-e}). \quad (4.1)$$

In the absence of the Yang-Lee edge (i.e., at criticality and in the ferromagnetic phase), we expect that a should be compatible with zero. At the critical point, Eq.(2.24) predicts that $c = \Delta/\nu$ and $e = \omega$. In the ferromagnetic regime, on the other hand, we expect $c = 3$ and $e = 1$. In the paramagnetic region, where the Yang-Lee edge is manifest, accurate estimates for the zeros should generate a non-vanishing value for a .

The FSS for the first four zeros at $T = T_c$ using the full magnetization ($|\mathbf{M}|$), through solving Eq.(2.10), is given in Fig. 3. A fit to the form (4.1) clearly points to a value $a \approx 0$.

L	$r_1(L)$	$r_2(L)$	$r_3(L)$	$r_4(L)$
8	0.00378744(2)	0.01136228(5)	0.01893702(8)	0.0265116(2)
12	0.001133597(3)	0.003400788(9)	0.00566797(2)	0.00793514(3)
16	0.0004806650(8)	0.001441994(2)	0.002403321(4)	0.003364646(6)
24	0.0001431430(2)	0.0004294297(6)	0.000715716(1)	0.001002002(2)
32	0.00006054220(4)	0.0001816267(2)	0.0003027111(2)	0.0004237954(3)
48	0.000017984100(9)	0.00005395236(3)	0.00008992060(5)	0.00012588883(7)
64	0.000007596710(4)	0.00002279013(1)	0.00003798356(2)	0.00005317698(3)

Table 3: The first four Lee-Yang zeros for different lattice sizes at $T = T_c/2$.

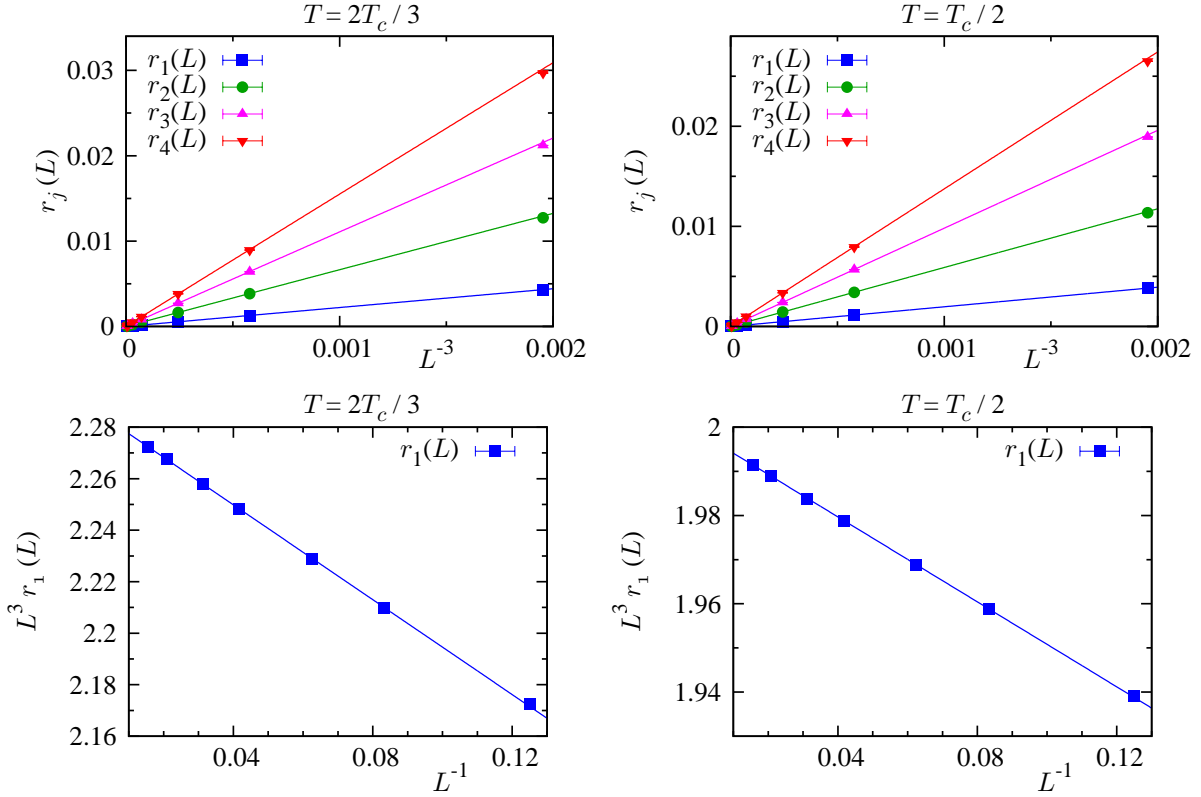


Figure 4: Scaling of the first four Lee-Yang zeros below the critical temperature (in color online). The upper panels confirm the leading finite-size scaling at the critical point as $\chi_L(0) \sim L^{-d} = L^{-3}$. The bottom panels confirm that the associated correction term is L^{-1} , indicative of the presence of Goldstone bosons.

Fixing this value for a and also fixing $e = \omega = 0.8$ leads to the estimates for Δ/ν listed in Table 5. All of the estimates are in agreement with the estimate $\Delta/\nu = 2.4805(4)$ coming

L	$r_1(L)$	$r_2(L)$	$r_3(L)$	$r_4(L)$
8	0.00424297(3)	0.012728664(8)	0.0212137(2)	0.0296977(2)
12	0.001278891(5))	0.001632521(8)	0.00639437(3)	0.00380919(2)
16	0.000544175(3)	0.0014419935(2)	0.00272086(2)	0.0033646459(6)
24	0.0001626250(4)	0.000487875(1)	0.000813124(2)	0.001138372(3)
32	0.0000689022(1)	0.0002067065(3)	0.0003445107(5)	0.0004823147(7)
48	0.00002050330(2)	0.00006150994(6)	0.0001025166(1)	0.0001435232(2)
64	0.000008668430(7)	0.00002600530(2))	0.00004334215(4)	0.00006067901(5)

Table 4: The first four Lee-Yang zeros for different lattice sizes at $T = 2T_c/3$.

from Ref. [5]. Fixing $f = 0$, on the other hand, leads to unacceptable fits. In this table we also present results whereby the zeros are obtained using just one of the individual components of the magnetization vector, in this case M_x . Clearly the scaling results do not depend on the selection of a specific component.

Next we study the FSS of the zeros below the critical temperature. The FSS behavior is plotted in Fig. 4. Again we obtain clear indications that $a = 0$, as expected. Again we do not obtain acceptable fits for the remaining scaling if we do not include a correction-to-scaling term. Fitting for both the leading and sub-leading behavior delivers the estimates listed Table 6. The leading scaling exponent is clearly equal to 3 in each case, and the correction exponents are very close to 1, indicating the presence of Goldstone modes, as discussed around Eq.(2.23).

We also investigate scaling with the index of the zeros, beginning with the ferromagnetic region. There, Eq.(2.24) predicts

$$\frac{r_j(L)}{r_1(L)} = \frac{j - \epsilon}{1 - \epsilon}. \quad (4.2)$$

This is also investigated in Fig.5 for two values of $T < T_c$. The two panels clearly indicate that r_j/r_1 is independent of T and of L . Moreover, their numerical values indicate that

$$\epsilon = \frac{1}{2} \quad \text{for } T < T_c. \quad (4.3)$$

Therefore the functional form involving the fractional number of zeros, previously suggested at criticality, extends to the ferromagnetic region too.

The j -dependency at the critical point is investigated in Fig.6. One observes that $r_j(L)/r_1(L)$ is also independent of L at T_c . The values of $r_j(L)/r_1(L)$ are, however, less easy to interpret than they were in the ferromagnetic case. The counterpart to Eq.(4.2) is

$$\frac{r_j(L)}{r_1(L)} = \left(\frac{j - \epsilon}{1 - \epsilon} \right)^{\frac{\Delta}{\nu d}} \left\{ 1 + \mathcal{O} \left(\frac{j - \epsilon}{L^d} \right)^{\frac{\omega}{d}} \right\}, \quad (4.4)$$

	$T = T_c$			
	$\langle \cos(r \mathbf{M}) \rangle = 0$		$\langle \cos(rM_x) \rangle = 0$	
	$c = \Delta/\nu$	χ^2/ndf	$c = \Delta/\nu$	χ^2/ndf
$r_1(L)$	2.4774(12)	0.11 / 2	2.4792(7)	2.57 / 5
$r_2(L)$	2.4789(28)	2.52 / 4	2.4845(17)	0.52 / 4
$r_3(L)$	2.4791(3)	5.36 / 4	2.4811(26)	0.89 / 5
$r_4(L)$	2.4793(4)	5.48 / 4	2.4779(52)	4.98 / 5

Table 5: Scaling exponent of the Lee-Yang zeros measured at the critical temperature. The estimates for the critical exponents are independent of the manner in which the zeros were determined, indicated by Eq.(2.10) and Eq.(2.11). ndf is the number of degrees of freedom of the fit.

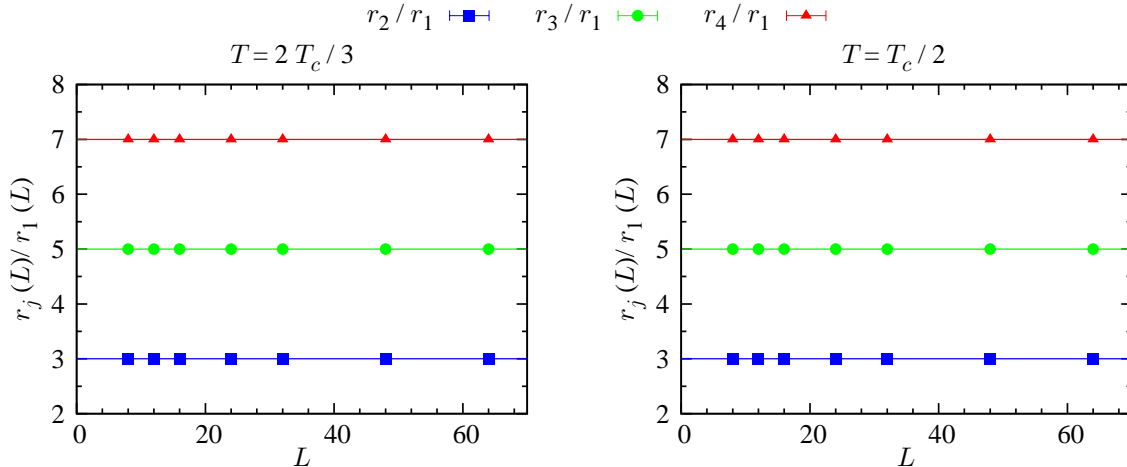


Figure 5: The ratio $r_j(L)/r_1(L)$ (in color online) is independent of L in the ferromagnetic phase and is, in fact, $2j - 1$.

and attempts to extract a precise estimate for ϵ from this formula are beset by large errors. Indeed, we cannot discount a functional dependency of ϵ on j . Instead the full dependency may be interpreted in terms of the density of zeros, and this is analyzed in Section 5.

Numerical determination of the locations of the Lee-Yang zeros in the paramagnetic phase is hampered by considerable limitations in algorithmic accuracy. In fact these problems are intrinsically so severe as to yield spurious zeros and hinder meaningful analysis of the Yang-Lee edge. For this reason, we relegate the discussion to the Appendix.

	$T = T_c/2$			$T = 2T_c/3$		
	c	e	χ^2/ndf	c	e	χ^2/ndf
$r_1(L)$	3.00024(8)	0.962(7)	2.98 / 2	3.0006(2)	0.949(8)	3.88 / 2
$r_2(L)$	3.00023(8)	0.963(7)	2.06 / 2	3.0005(2)	0.952(9)	3.68 / 2
$r_3(L)$	3.00022(8)	0.964(7)	1.78 / 2	3.0004(2)	0.956(9)	2.92 / 2
$r_4(L)$	3.00021(8)	0.965(7)	1.51 / 2	3.0003(2)	0.962(9)	1.84 / 2

Table 6: Scaling and correction to scaling exponents, c and e in Eq. (4.1), obtained from the Lee-Yang zeros below the critical temperature. The results confirm the prediction $c = d = 3$ and $e = 1$ from Eq.(2.24).

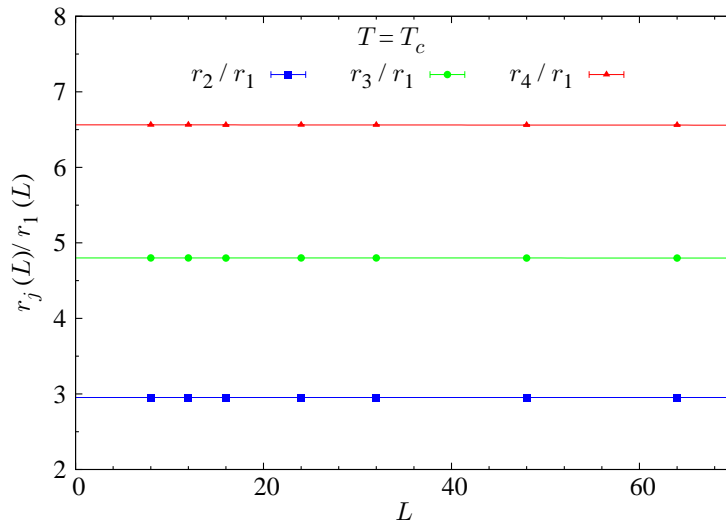


Figure 6: The ratio $r_j(L)/r_1(L)$ is independent of L also at the critical point (in color online).

5 Density of zeros

A numerical approach to the determination of the density of partition function zeros was developed in Refs.[14, 18]. The cumulative density for a finite-size system is defined as

$$G[r_j(T; L)] = \frac{2j - 1}{2L^d}. \quad (5.1)$$

At the infinite-volume critical point T_c this scales in the Lee-Yang case as

$$G(r) \sim r^{\frac{1}{\delta} + 1} = r^{\frac{\nu d}{\Delta}}, \quad (5.2)$$

which is compatible with the compact description of scaling given in subsection 2.2. In the ferromagnetic regime, on the other hand, one expects the linear behavior [14, 18]

$$G(r) \sim r. \quad (5.3)$$

Differentiating Eq.(5.2) gives a density of zeros $g(r) \sim r^{1/\delta}$, commensurate with the magnetic scaling form $m_\infty(T_c, h) \sim h^{\frac{1}{\delta}}$. Differentiating (5.3), on the other hand gives a

j	a_2	ω
1	1.2097(4)	0.9(3)
2	1.2094(3)	1.1(2)
3	1.2092(2)	1.23(6)
4	1.2090(3)	1.3(3)

Table 7: a_2 and ω from the density of zeros via Eq.(5.5).

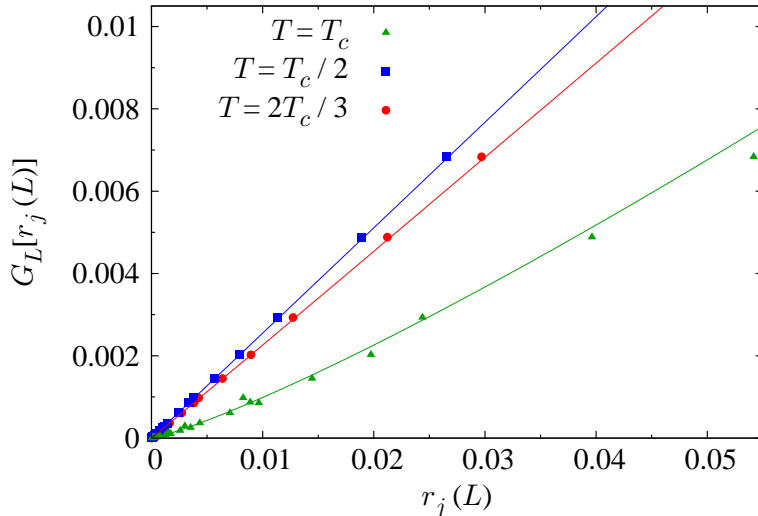


Figure 7: The density of zeros for at $T = T_c/2$ (denoted by the symbols \star , in blue online), $T = 2T_c/3$ (\times , green online) and at $T = T_c$ ($+$, red online).

non-vanishing density of zeros, ensuring a discontinuous transition across $h = 0$. Here, we wish to test these expectations for the 3D Heisenberg model. To do this, we fit our numerical data to the form

$$G_L[r_j(L)] = a_1[r_j(L)]^{a_2} + a_3, \quad (5.4)$$

where the coefficients depend on the temperature. We employ the fitting procedure used in Refs.[14, 18] whereby, in the absence of error bars for the density estimates in Eq.(5.1), one assumes an error of σ/L^d and then tunes σ to deliver a best fit with chi-squared per degree of freedom of one. This method delivers error estimates for the fitted parameters but precludes an independent goodness-of-fit test.

The data are plotted Fig. 7 for $T = T_c/2$, $T = 2T_c/3$ and $T = T_c$. Fitting to Eq.(5.4) yields $a_3 \approx 10^{-7} \pm 10^{-7}$ in each case. For the ferromagnetic data, fixing $a_3 = 0$ and fitting for the remaining parameters delivers a_2 compatible with 1 and supportive of Eq.(5.3). ($a_2 = 1.004(1)$ and $a_2 = 1.007(1)$ for $T = T_c/2$ and $T = 2T_c/3$, respectively when all data points are included in the fits, reducing to $a_2 = 1.001(1)$ and $a_2 = 1.002(1)$ when only the 8 points closest to the origin are used in the fits). At the critical point itself, using all data, one estimates $a_2 = 1.203(5)$. In comparison, the estimate $\eta = 0.0391(9)$ from Ref.[5] delivers $a_2 = \nu d/\Delta = 2d/(d + 2 - \eta) = 1.2095(2)$.

While the density plots give reasonable collapse in lattice sizes, we can also analyze each L independently for greater precision. In Table 7 we report the exponents we have obtained assuming a fit, including scaling corrections, of the form

$$r_j(L) = b_1 G_L^{b_2} (1 + b_3 G_L^{b_4}), \quad (5.5)$$

using error bars in $r_j(L)$ and not in G_L . With $a_2 = 1/b_2$ and $\omega = db_4$, we have also obtained reasonable agreement with the value $\omega \simeq 0.8$ quoted in the literature [6].

Finally, although there is no order parameter for the finite-size system, according to Lee and Yang’s fundamental theory of phase transitions, one can relate the density of zeros to the value of the spontaneous magnetization and one expects [7]

$$M_{\text{sp}} = \pi a_1. \tag{5.6}$$

We compare measurements of M_{sp} via Eq.(5.6) with direct estimates of $M_{\text{sp}} = \langle |\mathbf{M}| \rangle$, where \mathbf{M} is defined in Eq.(2.3). We perform the comparison using the full data sets for each $T < T_c$ as well as for each lattice size independently. We have checked that the data for each lattice follows a straight line according with the theoretical expectation and present our results in Table 8. We list in Table 8 the different estimates of the spontaneous magnetization for $T < T_c$ for the different lattice sizes. The agreement between them is excellent.

6 Conclusions

We have performed a numerical analysis of the Heisenberg model in three dimensions, paying special attention to the Lee-Yang zeros, the scaling properties of which contain information on Goldstone modes. Besides FSS for individual zeros in the critical and paramagnetic regimes, we have looked at the index of zeros and shown that a comprehensive description extends to both regions. These allow us to confirm very precise estimates for the critical exponents and correction terms. A first attempt to numerically examine scaling associated with the Yang-Lee edge in the paramagnetic region encounters obstacles which we elucidate directly and through analogy with the 1D Ising model. Finally, we confirm that study of the density of zeros for finite size, offers a compact way to investigate the onset of spontaneous magnetization, although the latter is only manifest in infinite volume.

Acknowledgments: This research was supported by Marie Curie International Incom-

L	M_{sp} measured directly		M_{sp} measured via density	
	$T = 2T_c/3$	$T = T_c/2$	$T = 2T_c/3$	$T = T_c/2$
8	0.723070(4)	0.810036(3)	0.723078(3)	0.810038(3)
12	0.710792(3)	0.801895(2)	0.710794(2)	0.801898(2)
16	0.704728(3)	0.797844(1)	0.7047315(20)	0.7978451(7)
24	0.698713(2)	0.793808(1)	0.6987122(8)	0.7938082(6)
32	0.695724(1)	0.791793(1)	0.6957245(5)	0.7917944(3)
64	0.691257(1)	0.7887771(4)	0.6912572(3)	0.7887785(2)

Table 8: Sample averaged spontaneous magnetization below the critical temperature measured directly and measured via Eq.(5.6) below the critical temperature using data for each lattice size individually.

ing Fellowship and International Research Staff Exchange Scheme grants within the 7th European Community Framework Program. AGG and JJR acknowledge support from Research Contracts No. FIS2007-60977 (MICINN), GR10158 (Junta de Extremadura) and PIRSES-GA-2011-295302 (European Union). RK thanks Nickolay Izmailian for discussions.

References

- [1] M.N. Barber, in Phase Transitions and Critical Phenomena, edited by C. Domb and J.L. Lebowitz (Academic, New York, 1983), Vol. 8.
- [2] M.H. Phan, V. Francoa, N.S. Bingham, H. Srikanth, N.H. Hur, S.C. Yu, Journal of Alloys and Compounds **508** (2010) 238244.
- [3] N. Dhahri, J. Dhahri, E.K. Hlil and E. Dhahri Journal of Magnetism and Magnetic Materials **324** (2012) 806.
- [4] M. Campostrini, M. Hasenbusch, A. Pelissetto, P. Rossi and E. Vicari, Phys. Rev. B **65**(2002) 144520.
- [5] A. Gordillo-Guerrero and J.J. Ruiz-Lorenzo, J. Stat. Mech. **P06014** (2007).
- [6] A. Pelissetto and E. Vicari, Phys. Rept. **368** (2002) 549 .
- [7] T.D. Lee and C.N. Yang, Phys. Rev. Lett. **87** (1952) 404; *ibid* **87** (1952) 410
- [8] F.Y. Wu, Talk given at Symposium in honor of Professor C. N. Yang's 85th birthday, Nanyang Technological University, Singapore, November 2007 (arXiv:1010.1838).
- [9] G. Gallavotti, S. Miracle-Sole and D.W. Robinson, Phys. Lett.A **25** (1967) 493; Commun. Math. Phys. **10** (1968) 311.
- [10] M.E. Fisher, Phys. Rev. Lett. **40** (1978) 1610.
- [11] T. Asano, Phys. Rev. Lett. **24** (1970) 1409.
- [12] J. J. Ruiz-Lorenzo, J. Phys. A **30**, 485 (1997).
- [13] C. Itzykson, R.B. Pearson and J.B. Zuber, Nucl. Phys. B **220** (1983) 415.
- [14] W. Janke and R. Kenna, J. Stat. Phys. **102**, 1211 (2001).
- [15] R.A. Baños, J.M. Gil-Narvion, J. Monforte-Garcia, J.J. Ruiz-Lorenzo and D. Yllanes, J. Stat. Mech. (2013) P02031.
- [16] H. G. Ballesteros, L. A. Fernández, V. Martín-Mayor, and A. Muñoz-Sudupe, Phys. Lett. B **387** (1996) 125.

[17] D.A. Kurtze and M.E. Fisher, J. Stat. Phys. **19** (1978) 205; Phys. Rev. B **20** (1979) 2785.

[18] W. Janke, D.A. Johnston and R. Kenna, Nucl. Phys. B 682 (2004) 618.

A spurious zeros in the paramagnetic phase

Fig. 8 shows the evolution of the expectation of the cosine in Eq.(2.11), through which the zeros are detected. One notices a remarkable difference between the amplitudes of the function below and above criticality; in the paramagnetic phase the amplitude of $\langle \cos(rM_x) \rangle$ is dampened as r increases, an effect not present at or below criticality. This leads to algorithmic detection of spurious Lee-Yang zeros in the symmetric phase.

That the detected zeros are indeed spurious is indicated firstly by a straightforward fit to Eq.(4.1), which delivers $a \approx 0$. The fact that the estimated zeros do not settle onto a Yang-Lee edge already hints that they are spurious. A second feature is that the scaling appears to indicate a leading exponent $c \approx 1.5 = d/2$. That this is also spurious is indicated as follows.

It is well known that the probability distribution of the magnetization in the paramagnetic phase follows an approximate Gaussian probability distribution. We write this distribution as (considering a single dimension here for simplicity)

$$P(M) = \frac{1}{\sqrt{2\pi V \chi_L^{(\text{nc})}}} \exp \left[-\frac{M^2}{2\chi_L^{(\text{nc})} V} \right], \quad (\text{A.1})$$

where M is the total magnetization, V is the volume and $\chi_L^{(\text{nc})} = \langle M^2 \rangle / V$ is the susceptibility, which is finite in the paramagnetic phase. The algorithm detects zeros through Eq.(2.11), and with the Gaussian distribution governing the high-temperature phase,

$$\langle \cos(rM) \rangle = \exp \left[-\frac{1}{2} \chi_L^{(\text{nc})} V r^2 \right] \quad (\text{A.2})$$

there. Here we have assumed $V \gg 1$ (otherwise this result would be modulated by an error-function factor). Therefore $\langle \cos(rM) \rangle$ decays exponentially quickly in the paramagnetic phase.¹ The reader can see the suitability of the Gaussian approximation in the inset of Fig. 8.

Numerically we compute $c(r) = \langle \cos(rM) \rangle$ with a given statistical error (which is also r -dependent) that we will denote $\delta(r)$. When $c(r_*) \sim \delta(r_*)$, a statistical fluctuation can induce a spurious zero at r_* . Hence, if we have similar error bars for all the lattice sizes, this implies, see Eq.(A.2), that the spurious zero scales as $1/\sqrt{V}$. This explains the origin

¹In $O(N)$ models one obtains:

$$\langle \cos(rM_x) \rangle = \exp \left[-\frac{1}{2N} \chi_L^{(\text{nc})} V r^2 \right]. \quad (\text{A.3})$$

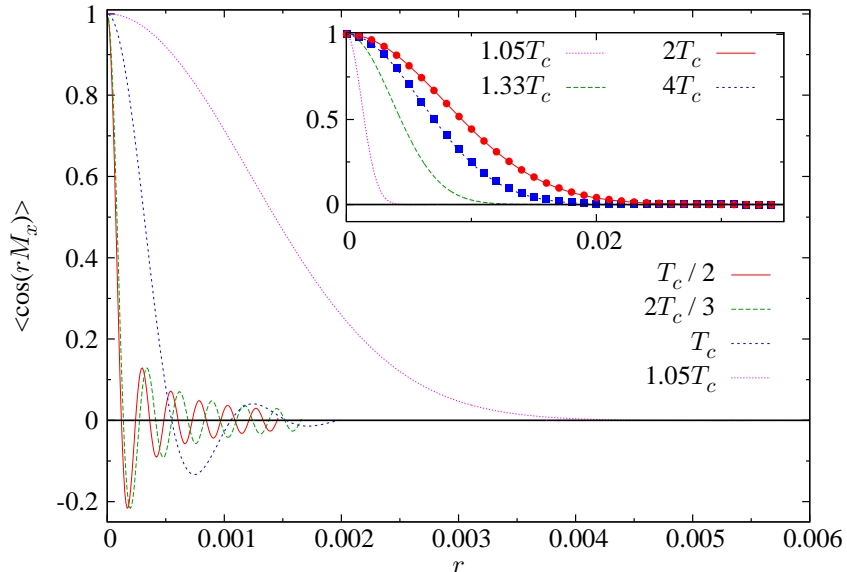


Figure 8: Behavior of $\langle \cos(rM_x) \rangle$ for the 3D Heisenberg model with $L = 32$ below, at, and above criticality (in color online). We have also plotted in the inset the behavior in the paramagnetic phase in order to show up the very different behavior there. In addition, we have plotted for the two highest temperatures the prediction from the Gaussian approximation (continuous lines), see Eq. (A.3), and the points (red and blue) from the numerical simulations: there are no free parameters, since we have used the susceptibility which was computed numerically. Notice the good agreement. For $T = 1.05T_c$ and $T = 1.33T_c$ we only show the data from numerical simulations (dashed lines).

and scaling of the spurious paramagnetic zeros – The behavior is simply due to finite statistics associated with the numerical approach. Instead, if we improve the statistics, reducing the value of $\delta(r_*)$, the spurious zero should disappear.

We can gain further insight by examining slope of $\langle \cos(rM) \rangle$, which is

$$\frac{d}{dr} \langle \cos(rM) \rangle = -\langle M \sin(rM) \rangle. \quad (\text{A.4})$$

We can examine this slope in the three different regimes. At and below the critical point, we use the fact that $M \simeq \sqrt{\langle M^2 \rangle}$, to see that in both cases $r_1 M$ is $O(1)$, where r_1 is a genuine zero (and having used the scaling of the zeros in each of these two regions). Therefore, close to r_1 ,

$$\left. \frac{d}{dr} \langle \cos(rM) \rangle \right|_{r_1} \sim |M|. \quad (\text{A.5})$$

Since $|M| \sim V$ in the ferromagnetic phase, and its typical value at criticality is $|M| \simeq \sqrt{\langle M^2 \rangle} = \sqrt{V \chi_L^{(\text{nc})}}$, it is clear that at and below the critical temperature the slope is large. Since the algorithm detects zeros through changes in the sign of $\langle \cos(rM) \rangle$, it is

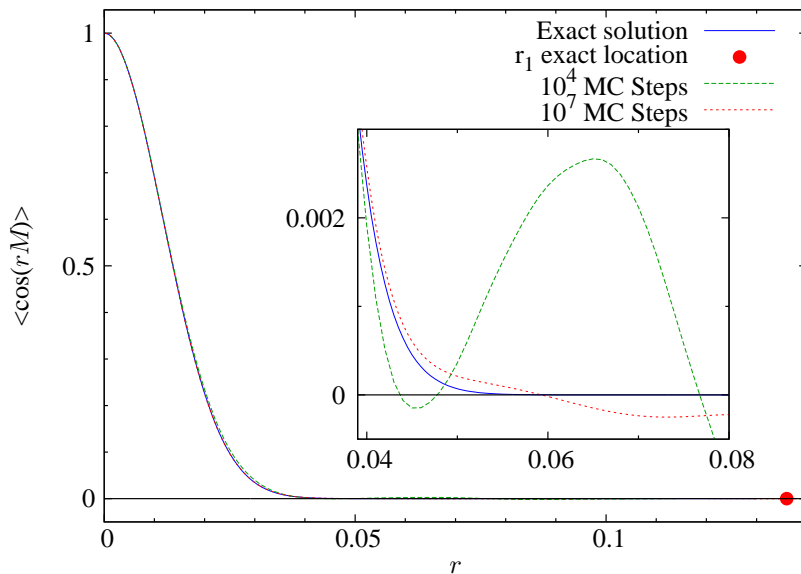


Figure 9: Behavior of $\langle \cos(rM) \rangle$ for the 1D Ising model with $L = 1000$ above criticality, i.e., above $T = 0$ (in color online). The exact zero is indicated by the red disc and the exact solution by a blue line. The numerical algorithm, however, detects spurious zeros as can be seen in the inset.

robust in the critical and ferromagnetic regions. In the paramagnetic region, however, the Gaussian approximation gives

$$\left. \frac{d}{dr} \langle \cos(rM) \rangle \right|_{r_1} = -r_1 V \chi \exp \left[-\frac{1}{2} \chi V r_1^2 \right]. \quad (\text{A.6})$$

This gives an exponentially depressed slope in the paramagnetic phase, rendering detection of genuine zeros difficult and spurious zeros (as noise) feasible.

To check the above interpretation, we refer to the Ising model in one dimension, where the partition function in a magnetic field can be analytically determined using periodic boundary conditions and where the entire $T > 0$ region is paramagnetic [7]. The two eigenvalues of the transfer matrix are

$$\lambda_{\pm}(\beta, H) = e^{\beta} \left[\cosh(H) \pm \sqrt{e^{-4\beta} + \sinh^2(H)} \right], \quad (\text{A.7})$$

and the partition function of a chain of L spins is

$$Z(\beta, H) = \lambda_+(\beta, H)^L + \lambda_-(\beta, H)^L. \quad (\text{A.8})$$

Introducing a pure imaginary magnetic field by defining $H = ir$, the eigenvalues can be written

$$\lambda_{\pm}(\beta, ir) = e^{\beta} \left[\cos(r) \pm \sqrt{e^{-4\beta} - \sin^2(r)} \right]. \quad (\text{A.9})$$

Notice that for $e^{-2\beta} < \sin^2(r)$, the eigenvalues, λ_{\pm} , are complex numbers but satisfying $\lambda_+^* = \lambda_-$. This confirms our earlier statement that the partition function in a pure imaginary magnetic field is real. One finds [17]

$$\langle \cos(rM) \rangle = \frac{Z(\beta, ir)}{Z(\beta, 0)} = \frac{\lambda_+(\beta, ir)^L + \lambda_-(\beta, ir)^L}{\lambda_+(\beta, 0)^L + \lambda_-(\beta, 0)^L}. \quad (\text{A.10})$$

Therefore the zeros in the paramagnetic phase of the one-dimensional Ising model can be exactly determined. In Fig. 9, the first zero for such a system is depicted as a disc (red online). This figure also depicts the results for $\langle \cos(rM) \rangle$ from two Monte Carlo simulations and for the exact solution. As expected, the numerically computed $\langle \cos(rM) \rangle$ decays rapidly with increasing r , it then remains very close to zero and traverses the axis well before the true zero is reached (green line). Although the situation improves with increased numerical accuracy (see red line), the figure clearly demonstrates that the Lee-Yang edge is not reliably accessible using this numerical technique.